SARS-CoV-2 E and 3a Proteins Are Inducers of Pannexin Currents

Barbara Oliveira-Mendes, Malak Alameh, Béatrice Ollivier, Jérôme Montnach, Nicolas Bidère, Frédérique Souazé, Nicolas Escriou, Flavien Charpentier, Isabelle Baró, Michel de Waard, et al.

cells

MDPI

Article

SARS-CoV-2 E and 3a Proteins Are Inducers of Pannexin Currents

Barbara B. R. Oliveira-Mendes [1,†], Malak Alameh [1,2,†], Béatrice Ollivier [1], Jérôme Montnach [1], Nicolas Bidère [3,4], Frédérique Souazé [5], Nicolas Escriou [6], Flavien Charpentier [1], Isabelle Baró [1], Michel De Waard [1,2,*,‡] and Gildas Loussouarn [1,*,‡]

1 L'institut du Thorax, Nantes Université, CNRS, INSERM, F-44000 Nantes, France; barbara.ribeiro@univ-nantes.fr (B.B.R.O.-M.); malak.alameh@univ-nantes.fr (M.A.)
2 Labex Ion Channels, Science and Therapeutics, F-06560 Valbonne, France
3 Team SOAP, CRCI2NA, INSERM, CNRS, Nantes Université, Université d'Angers, F-44000 Nantes, France
4 Equipe Labellisée Ligue Contre le Cancer, F-75006 Paris, France
5 CRCI2NA INSERM, CNRS, Nantes Université, F-44000 Nantes, France
6 Institut Pasteur, Université Paris Cité, Département de Santé Globale, F-75015 Paris, France
* Correspondence: michel.dewaard@univ-nantes.fr (M.D.W.); gildas.loussouarn@univ-nantes.fr (G.L.); Tel.: +33-228-080-076 (M.D.W.)
† These authors contributed equally to this work.
‡ These authors contributed equally to this work.

Abstract: Controversial reports have suggested that SARS-CoV E and 3a proteins are plasma membrane viroporins. Here, we aimed at better characterizing the cellular responses induced by these proteins. First, we show that expression of SARS-CoV-2 E or 3a protein in CHO cells gives rise to cells with newly acquired round shapes that detach from the Petri dish. This suggests that cell death is induced upon expression of E or 3a protein. We confirmed this by using flow cytometry. In adhering cells expressing E or 3a protein, the whole-cell currents were not different from those of the control, suggesting that E and 3a proteins are not plasma membrane viroporins. In contrast, recording the currents on detached cells uncovered outwardly rectifying currents much larger than those observed in the control. We illustrate for the first time that carbenoxolone and probenecid block these outwardly rectifying currents; thus, these currents are most probably conducted by pannexin channels that are activated by cell morphology changes and also potentially by cell death. The truncation of C-terminal PDZ binding motifs reduces the proportion of dying cells but does not prevent these outwardly rectifying currents. This suggests distinct pathways for the induction of these cellular events by the two proteins. We conclude that SARS-CoV-2 E and 3a proteins are not viroporins expressed at the plasma membrane.

Keywords: COVID-19; SARS-CoV-2; viroporins; E protein; 3a protein; pannexin currents; cell death

Citation: Oliveira-Mendes, B.B.R.; Alameh, M.; Ollivier, B.; Montnach, J.; Bidère, N.; Souazé, F.; Escriou, N.; Charpentier, F.; Baró, I.; De Waard, M.; et al. SARS-CoV-2 E and 3a Proteins Are Inducers of Pannexin Currents. *Cells* **2023**, *12*, 1474. https://doi.org/10.3390/cells12111474

Academic Editor: Mahmoud Huleihel

Received: 13 March 2023
Revised: 10 May 2023
Accepted: 18 May 2023
Published: 25 May 2023

1. Introduction

SARS-CoV-2 is the third virus of the genus Beta-coronavirus of the Coronaviridae family to be responsible for a Severe Acute Respiratory Syndrome in this century, after SARS-CoV-1 in 2002–2003 [1] and MERS-CoV in 2012 [2]. As a result, it is of great importance to best characterize the coronaviruses and their associated pathophysiologies, with the hope that new treatments will emerge to complement vaccine approaches for people who cannot access the vaccines or are not responsive to them. In addition to Paxlovid which is already available but associated with bothersome side-effects [3], many potential anti-COVID-19 treatments are in development, but it is too soon to tell how efficient they will be, namely with regard to the continuous emergence of new variants, and if their cost will be reasonable [4].

Viroporins, i.e., ion channels encoded by a virus genome, are potential targets for antiviral agents, as demonstrated by the case of amantadine, which inhibits the acid-activated M2 channel of the Influenza A virus [5]. Several studies led to the suggestion that two proteins of SARS-CoV are viroporins. The SARS-CoV-2 Envelop (E) protein is a one-transmembrane-domain membrane protein (75 amino-acids) almost identical to the SARS-CoV-1 Envelop protein (95% identity). The SARS-CoV-2 ORF3a (3a) protein is a larger three-transmembrane-domain membrane protein (275 amino-acids) relatively similar to the SARS-CoV-1 3a protein (73% identity).

Regarding the ion channel function of these proteins, there are clearly several contradicting studies: some of them raising intriguing issues, while others do not confirm these reports. Concerning in vitro membrane incorporation of purified E or 3a protein in lipid bilayers, the presence of ion channel activity is reportedly associated with these viral proteins [6–11]. However, a review article soundly outlined the lack of robust data and raised ethical concerns, casting doubts on the validity of these scientific messages [12]. Concerning viral protein expression in cells, the expression of SARS-CoV-1 E protein also led to conflicting results [13,14]. Pervushin et al. managed to identify plasma membrane currents generated by heterologous expression of SARS-CoV-1 E protein in HEK-293 cells [13], but not Nieto-Torres et al. [14]. In Pervushin's study, the strongest evidence for E protein expression at the plasma membrane forming ion channels was the finding that (i) hexamethylene amiloride (HMA) inhibits the induced current and (ii) directly binds to the E protein. A recent study also detected current after injection in *Xenopus laevis* oocytes of any RNA among four different RNAs encoding SARS-CoV-2 proteins, including the E protein [15]. On the other hand, in other studies, expression of SARS-CoV-2 E protein did not lead to interpretable ionic currents in HEK-293S cells or *Xenopus laevis* oocytes [16,17]. In an attempt to favor plasma membrane targeting and reveal a putative current, a C-terminal predicted ER retention signal of SARS-CoV-2 E protein was replaced by a Golgi export signal from the Kir2.1 channel. The expression of this chimera could then be associated with the generation of a non-rectifying and cation-selective current [16]. This current was thus quite different from the outwardly rectifying current observed by Pervushin and collaborators [13]. Furthermore, another study using a membrane targeting sequence, fused to the N-terminus of the SARS-CoV-1 E protein, provided a non-rectifying current that was 100-fold larger than the one observed in the two previous studies [18]. This suggests that such modifications of either the N- or C-terminus are too drastic to faithfully report the actual activity of the native proteins.

The SARS-CoV 3a protein was also investigated. Confocal immuno-imaging detected the expression of WT 3a protein in both plasma membrane and cytoplasm. Membrane expression was reduced for a mutant that showed less current when expressed in HEK-293 cells [19]. Expression of the wild-type (WT) protein in HEK-293 cells but also *Xenopus laevis* oocytes was associated with a poorly selective outwardly rectifying current in both models, resembling the one observed upon expression of the E protein [15,20–22]. However, again, these observations were not replicated by other laboratories [23].

To summarize, there is no unequivocal evidence that SARS-CoV E and 3a proteins are viroporins active at the plasma membrane of the host cell. However, on one hand, it was recently reported that SARS-CoV-2 E and 3a proteins can promote cell death [24,25]. On the other hand, apoptosis is associated with an increase in the outwardly rectifying current conducted by pannexins [26–28] and VRAC channels [29]. This led us to reinvestigate the actual function(s) of SARS-CoV-2 E and 3a proteins in mammalian cells in the frame of the cell toxicity of these proteins.

In this study, CHO cells expressing either CoV-2 E or 3a proteins tended to develop a round-shaped form with a tendency to detach from the Petri dish, a process exacerbated compared to control conditions. This cell phenotype is consistent with cell death [30,31] and we confirmed via flow cytometry experiments that expression of E or 3a proteins does indeed promote cell death. Transfected cells, still attached to the Petri dish (adhering cells), had unchanged basal currents, indicating that E and 3a proteins are unlikely to

act as plasma membrane channels. In contrast, recording whole-cell currents on round-shaped and detached cells, we observed large outwardly rectifying currents only in E or 3a protein-expressing cells but not in control dying cells. This current is reminiscent of those observed in previous publications using HEK-293 cells and oocytes expressing SARS-CoV-1 proteins [13,20–22]. The application of carbenoxolone and probenecid, two inhibitors of pannexin channels, suggests for the first time that these currents are pannexin-mediated conductances, potentially activated by altered morphology or apoptosis. In conclusion, both SARS-CoV-2 E and 3a proteins are most likely triggers of endogenous conductance.

2. Materials and Methods

2.1. Cell Culture

The Chinese Hamster Ovary cell line, CHO, was obtained from the American Type Culture Collection (CRL-11965, Manassas, VA, USA) and cultured in Dulbecco's modified Eagle's medium (Gibco 41966-029, Gaithersburg, MD, USA) supplemented with 10% fetal calf serum (Eurobio, Les Ulis, France), 2 mM L-Glutamine and antibiotics (100 U/mL penicillin and 100 µg/mL streptomycin, Corning, NY, USA) in 5% CO_2, maintained at 37 °C in a humidified incubator. This cell line was confirmed to be mycoplasma-free (MycoAlert, Lonza, Basel, Switzerland).

2.2. Drugs

Carbenoxolone disodium salt was purchased from Sigma (St. Louis, MO, USA), and a 100 mmol/L stock solution was prepared in H_2O. Probenecid was purchased from Sigma, and a 200 mmol/L stock solution was prepared in DMSO. The drugs used for the flow cytometry experiments were QVD-OPh (#OPH001, R&D Systems, Minneapolis, MN, USA, 10 mmol/L stock solution in DMSO), S63-845 (Chemietek, Indianapolis, IN, USA, 10 mmol/L stock solution in DMSO), and ABT737 (Selleckchem, Houston, TX, USA, 10 mmol/L stock solution in DMSO).

2.3. Construction of E and 3a Protein-Encoding Plasmids

SARS-CoV-2 E and 3a nucleotide sequences containing a Kozak sequence added right before the ATG (RefSeq NC_045512.2) were synthesized by Eurofins (Ebersberg, Germany) and subcloned into the pIRES2 vector with eGFP in the second cassette (Takara Bio Europe, Saint-Germain-en-Laye, France). Truncated Δ4 and Δ8 E proteins as well as Δ10 3a protein constructs lacking the last 12, 24, and 30 nucleotides, respectively, were also synthesized by Eurofins. The plasmid cDNAs were systematically re-sequenced by Eurofins after each plasmid in-house midiprep (Qiagen, Hilden, Germany).

2.4. E and 3a cDNA Transfection

Fugene 6 transfection reagent (Promega, Madison, WI, USA) was used to transfect WT and mutant E and 3a plasmids for patch clamp, morphology analysis, and flow cytometry experiments according to the manufacturer's protocol. The cells were cultured in 35 mm dishes and transfected at 20% confluence for patch clamp experiments and 50% confluence for flow cytometry assays, with a pIRES plasmid (2 µg DNA) with the first cassette empty or containing wild-type or truncated SARS-CoV-2 E or 3a protein sequences. For morphology analysis, cells were cultured in ibidi µ-Slide 8-well dishes and transfected at 20% confluence with the same plasmids. In pIRES2-eGFP plasmids, the second cassette (eGFP) is less expressed than the first cassette, guaranteeing the expression of a high level of the protein of interest in fluorescent cells [32,33].

2.5. Electrophysiology

Two days after transfection, the CHO cells were mounted on the stage of an inverted microscope and bathed with a Tyrode solution (in mmol/L: NaCl 145, KCl 4, $MgCl_2$ 1, $CaCl_2$ 1, HEPES 5, glucose 5, pH adjusted to 7.4 with NaOH) maintained at 22.0 ± 2.0 °C. Patch pipettes (tip resistance: 2.0 to 2.5 MΩ) were pulled from soda-lime glass capil-

laries (Kimble-Chase, Vineland, NJ, USA) with a Sutter P-30 puller (Novato, CA, USA). A fluorescent cell was selected via epifluorescence. The pipette was filled with intracellular medium containing (in mmol/L): KCl, 100; Kgluconate, 45; $MgCl_2$, 1; EGTA, 5; HEPES, 10; pH adjusted to 7.2 with KOH. Stimulation and data recording were performed with pClamp 10, an A/D converter (Digidata 1440A), and a Multiclamp 700B (all Molecular Devices, San Jose, CA, USA) or a VE-2 patch-clamp amplifier (Alembic Instruments, Montreal, QC, Canada). The currents were acquired in the whole-cell configuration, low-pass filtered at 10 kHz and recorded at a sampling rate of 50 kHz. First, a series of twenty 30-ms steps to −80 mV was applied using alternating holding potential (HP) values of −70 mV and −90 mV, and Cm and Rs values were subsequently calculated offline from the recorded currents. The currents were then recorded using a 1-s ramp protocol from −80 mV to +70 mV every 4 s. Regarding non-adhering cells, we considered them as having large current density when the current density measured at +70 mV was superior to mean + 2 × standard deviation of the current density in adhering cells in the same condition.

2.6. Cell Morphology Assay

Cell roundness was estimated using the *Analyze Particle* function of the Fiji software (v 1.53), as described in Supplementary Figure S1.

2.7. Flow Cytometry Assay

Two days after transfection, the CHO cells were prepared for cell death detection following the user guide (https://assets.thermofisher.com/TFS-Assets/LSG/manuals/mp13199.pdf, accessed on 2 February 2021) to measure annexin V binding and propidium iodide (PI) intake. The cells were washed with cold PBS, trypsinized, collected via centrifugation and gently resuspended in annexin-binding buffer (V13246, Invitrogen, Carlsbad, CA, USA) at 1×10^6 cells/mL. To each 300 µL cell suspension were added 0.5 µL of annexin V AlexaFluor 647 (A23204, Invitrogen, Carlsbad, CA, USA) and 1 µL of propidium iodide (PI) at 100 µg/mL (P3566, Invitrogen, Carlsbad, CA, USA). The CHO cells were incubated at room temperature for 15 min in the dark, then maintained on ice until flow cytometry analysis within one hour.

To study the cell death pathways induced by E and 3a protein expression, non-transfected or transfected CHO cells were treated with inhibitors or inducers of apoptosis (inhibitor: 5 µmol/L QVD-OPh incubated for 48 h; activators: 3 µmol/L S63-845 + 8 µmol/L ABT737 incubated for 3 h).

The cytometer BD FACSCanto (BD Biosciences, Franklin Lakes, NJ, USA) was used to sample acquisition. CHO cells transfected with an empty plasmid were used to determine the population to be analyzed. Monolabeled cells were used to establish the photomultiplier voltage of each channel (PMT) and proceed with fluorescence compensation after the acquisitions. In order to detect cell death, only eGFP-positive CHO cells (FITC) were selected to study Annexin V AlexaFluor 647 (APC) and PI (Perc-P) labeling. The analyses were performed using FlowJo software (v10.7.1).

3. Results

We first focused on native E and 3a proteins. To maximize the chance of observing E and 3a protein-induced ionic currents, we chose to use pIRES plasmids, in which the protein of interest situated in the first cassette is more expressed than the eGFP reporter in the second cassette, thereby guaranteeing the expression of a high level of the protein of interest in fluorescent cells [32,33]. For the purpose of this study, we also selected CHO rather than HEK-293 cells because they express minimal endogenous currents [34]. We compared whole-cell currents recorded during a ramp protocol in cells transfected either with a control pIRES2-eGFP plasmid (pIRES) or the same plasmid containing the cDNA of the SARS-CoV-2 E protein (pIRES–E) or 3a protein (pIRES–3a). Unexpectedly, we did not observe any difference in the currents recorded for the SARS-CoV-2 protein-expressing cells compared to the control pIRES condition (Figure 1A). However, many cells transfected with

either E- or 3a-encoding plasmids developed altered morphology, shifting from spindle-like cells to more round cells (Figure 1B), similar to what was previously observed in MDCK cells heterologously expressing SARS-CoV-1 E protein [35]. Morphology analysis with a Fiji tool confirmed an increase in cell roundness (Figure 1C and Supplementary Figure S1). In particular, in the patch clamp experiments, some cells were coming off from the dish bottom because of loss of adhesion. Cell counting indicated that slightly more cells were losing adhesion when E or 3a proteins were expressed (3.4 ± 0.6% in non-transfected cells, 5.2 ± 1.0% in pIRES condition, 6.6 ± 0.7% in pIRES–E, $p < 0.001$ vs. pIRES, 6.0 ± 1.2% in pIRES–3a, $p < 0.001$ vs. pIRES, five replicates, *z*-test). As is standard, the currents shown in Figure 1A were recorded from the adhering cells, while the non-adhering cells were disregarded in this initial investigation. Noteworthily, in each condition, both spindle-like and round adhering cells were studied (pIRES: 21 spindle-like and 17 round cells; pIRES E: 9 and 13, pIRES 3a: 18 and 11).

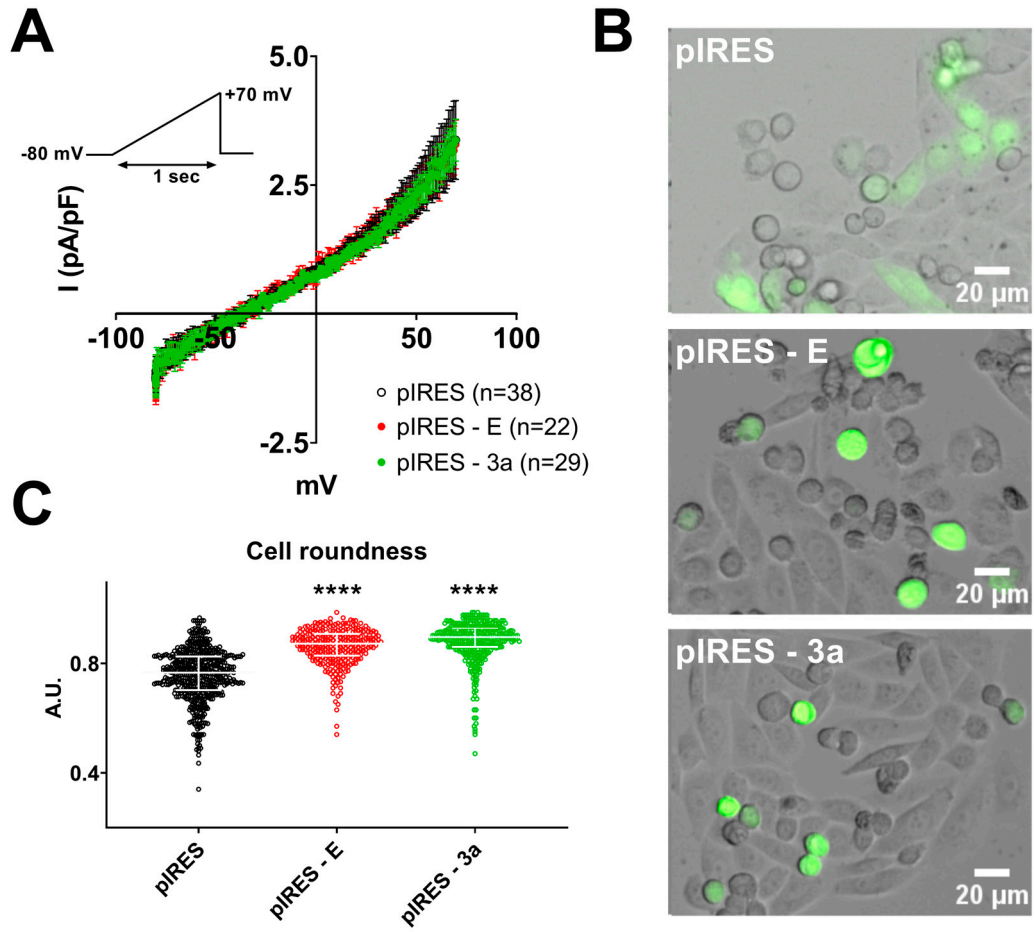

Figure 1. Expression of E or 3a protein is accompanied by altered cellular morphology but no modification in whole-cell currents in adhering cells. (**A**) Average current densities (±sem) recorded during the ramp protocol (inset) in adhering CHO cells expressing either only eGFP (pIRES), SARS-CoV-2 E and eGFP proteins (pIRES–E), or SARS-CoV-2 3a and eGFP proteins (pIRES–3a). (**B**) Superimposed brightfield and eGFP fluorescence images of CHO cells in the same 3 conditions as shown in A. (**C**) Morphology analysis, cf. Supplementary Figure S1. Plot of individual cells (pIRES, n = 1922; pIRES–E, n = 1198; and pIRES–3a, n = 1283), median ± interquartile range. ****: $p < 0.0001$ as compared to pIRES control, Kruskal-Wallis test.

Since both E and 3a proteins promote cell death [24,25], we hypothesized that the various cell morphological patterns (spindle-shaped, round-adhering, and round non-adhering) may correspond to the development of cell death, as described earlier in CHO and other cells [30,31]. The flow cytometry analysis performed on the eGFP-positive CHO cells

(Figure 2) showed that expression of E and 3a proteins increases the percentage of dying cells, with more significantly late cell death, revealed by propidium iodide permeability (Supplementary Figure S2). The effect of 3a protein was greater than the effect of E protein. E protein-induced cell death could be reduced by the pan-caspase inhibitor QVD-OPh, while 3a protein-induced cell death could not (Supplementary Figures S3 and S4), suggesting that E protein induces apoptosis, while 3a protein activates non-conventional caspase-independent cell death.

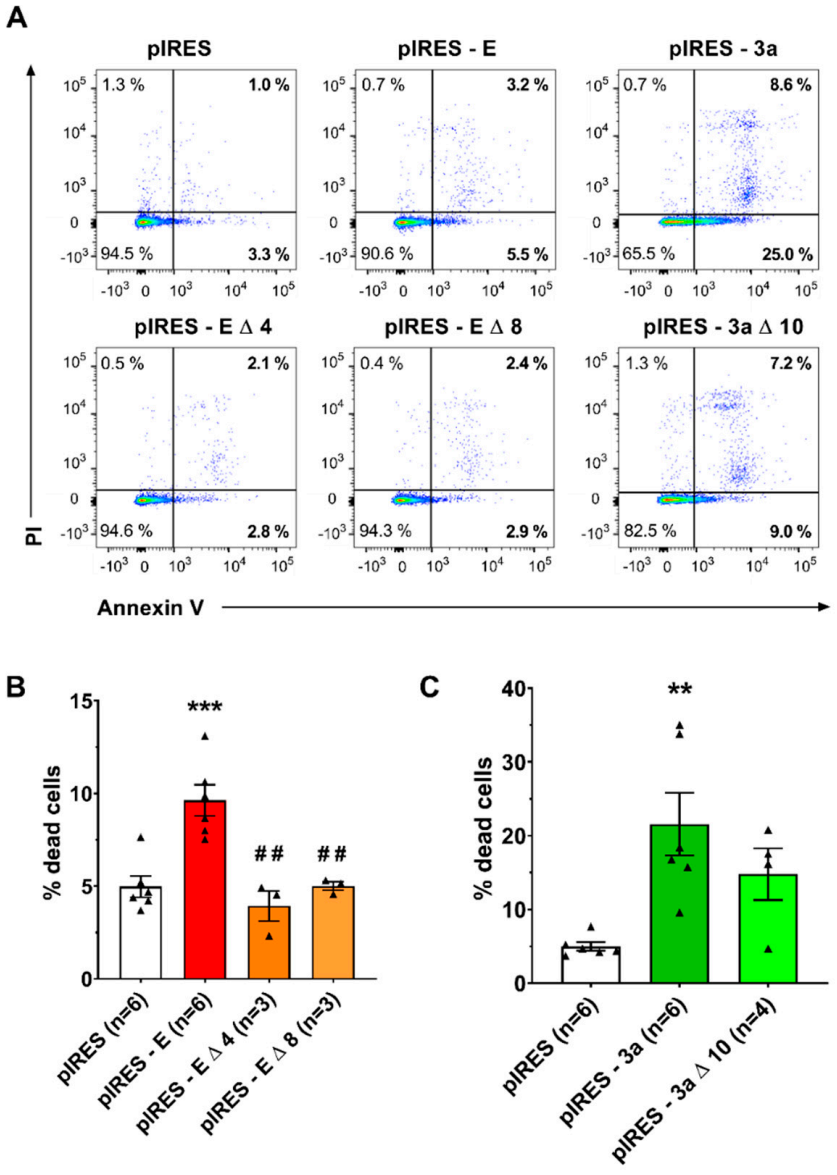

Figure 2. Expression of E and 3a protein induces cell death. (**A**) Flow cytometry analysis of eGFP-positive CHO cells expressing only eGFP (pIRES) or co-expressing eGFP and one of the following SARS-CoV-2 proteins: the full-length E protein (pIRES–E), C-terminally deleted E proteins (pIRES–E Δ 4 or pIRES–E Δ 8), full-length 3a protein (pIRES–3a) or C-terminally deleted 3a protein (pIRES–3a Δ 10). After 48 h of expression, cells were stained with annexin V AlexaFluor 647 (APC)/propidium iodide (PI, Perc-P). (**B**) Mean percentage (±sem) of Annexin V+ cells among eGFP-positive CHO cells expressing only eGFP (pIRES) or eGFP and full-length or truncated E protein. ***: $p < 0.001$ as compared to pIRES control, one-way ANOVA, ##: $p < 0.01$ as compared to E protein, *t*-test. (**C**) Mean percentage (±sem) of Annexin V+ cells among eGFP-positive CHO cells expressing only eGFP (pIRES), or eGFP and full-length or truncated 3a protein. **: $p < 0.01$ as compared to pIRES control, one-way ANOVA.

Both E and 3a proteins possess a C-terminal PDZ binding motif (PBM). E-protein PBM has been suggested to be a virulence factor [11] that binds to host cell PDZ domains, leading to abnormal cellular distribution of the bound proteins [35]. 3a PBM interacts with at least five human PDZ-containing proteins (TJP1, NHERF3 and 4, RGS3, PARD3B), suggesting that it also alters cellular organization [36]. We thus evaluated whether deletion of these domains impacts the propensity of E and 3a proteins to trigger cell death. Two C-terminal deletions used in previous studies to remove E protein PBM, Δ4 for the last four amino acids [35] and Δ8 for the last eight residues [11], abolished the pro-apoptotic effect of E protein (Figure 2). When looking individually at early and late cell death, we observed that both truncations of E and 3a protein decreased late cell death (Supplementary Figure S2).

Since both E and 3a proteins promote altered morphology and cell death, we hypothesized that the cells starting to come off the surface may express currents induced by altered morphology and/or cell death, such as volume-regulated anion channel (VRAC) or pannexin currents [26–29,37,38]. We thus compared patch clamp recordings of adhering cells vs. non-adhering cells for three conditions: control pIRES, pIRES–E and pIRES–3a plasmids (Figure 3). For the control pIRES condition, focusing on non-adhering cells in the 35 mm dish and using the ramp protocol, we observed an outwardly rectifying current with a mean current density of 8.5 ± 3.1 pA/pF at +70 mV, slightly higher than those of spindle- or round-shaped adhering cells (3.4 ± 0.8 pA/pF). On the other hand, in non-adhering cells expressing either the E or 3a protein, currents were much larger in the E protein condition (I_{+70mV} = 31 ± 9 pA/pF, two-way ANOVA test on the ramp-evoked currents: $p < 0.0001$) and the 3a protein condition (I_{+70mV} = 44 ± 13 pA/pF, two-way ANOVA test on the ramp-evoked currents: $p < 0.0001$) compared to non-adhering cells in the control pIRES condition. Noteworthily, only a fraction of the non-adhering cells exhibited large rectifying currents, as shown in Figure 3: 4 out of 43 in the control pIRES condition, 14 out of 46 in the E protein condition, and 16 out of 41 in the 3a protein condition. These experiments suggest that changes in morphology and/or cell death induced by expression of E and 3a proteins may lead to an increased membrane permeability by enhancing the expression or activity of an endogenous ion channel.

Current density is classically used to compare channel activity in single cells, but since cell morphology is affected by the expression of E and 3a proteins, we tested if membrane capacitance is modified in non-adhering cells. Supplementary Figure S5 actually shows a reduction in membrane capacitance in non-adhering cells in several conditions. In order to verify that the increase in current density observed in non-adhering cells in Figure 3 is not indirectly due to the decrease in membrane capacitance, we also compared the current amplitudes (not divided by membrane capacitance) and still observed significantly larger rectifying currents when E or 3a protein was expressed (Supplementary Figure S6).

The outwardly rectifying currents that we observed resemble both VRAC currents conducted by swelling activated anion channels and pannexin currents that are not only apoptosis-induced but also stretch-induced [26–29,37,38]. We chose carbenoxolone (CBX), which inhibits both channels with similar affinity [39,40], and applied it on non-adhering cells that display large outwardly rectifying currents (Figure 4). We observed that CBX, applied at 50 µmol/L, inhibits the observed current, restoring current amplitudes similar to the ones observed in the control cells. Probenecid is commonly used to inhibit pannexin channels and seems quite specific for pannexin currents, showing little effect on connexin channels and no described effect on VRAC channels [40,41]. We observed that probenecid, applied at 300 µmol/L, also inhibits the large outwardly rectifying currents observed in the non-adhering E protein expressing cells (Figure 5). Altogether, these observations suggest that the current triggered by the expression of E and 3a proteins is most probably conducted by pannexin channels.

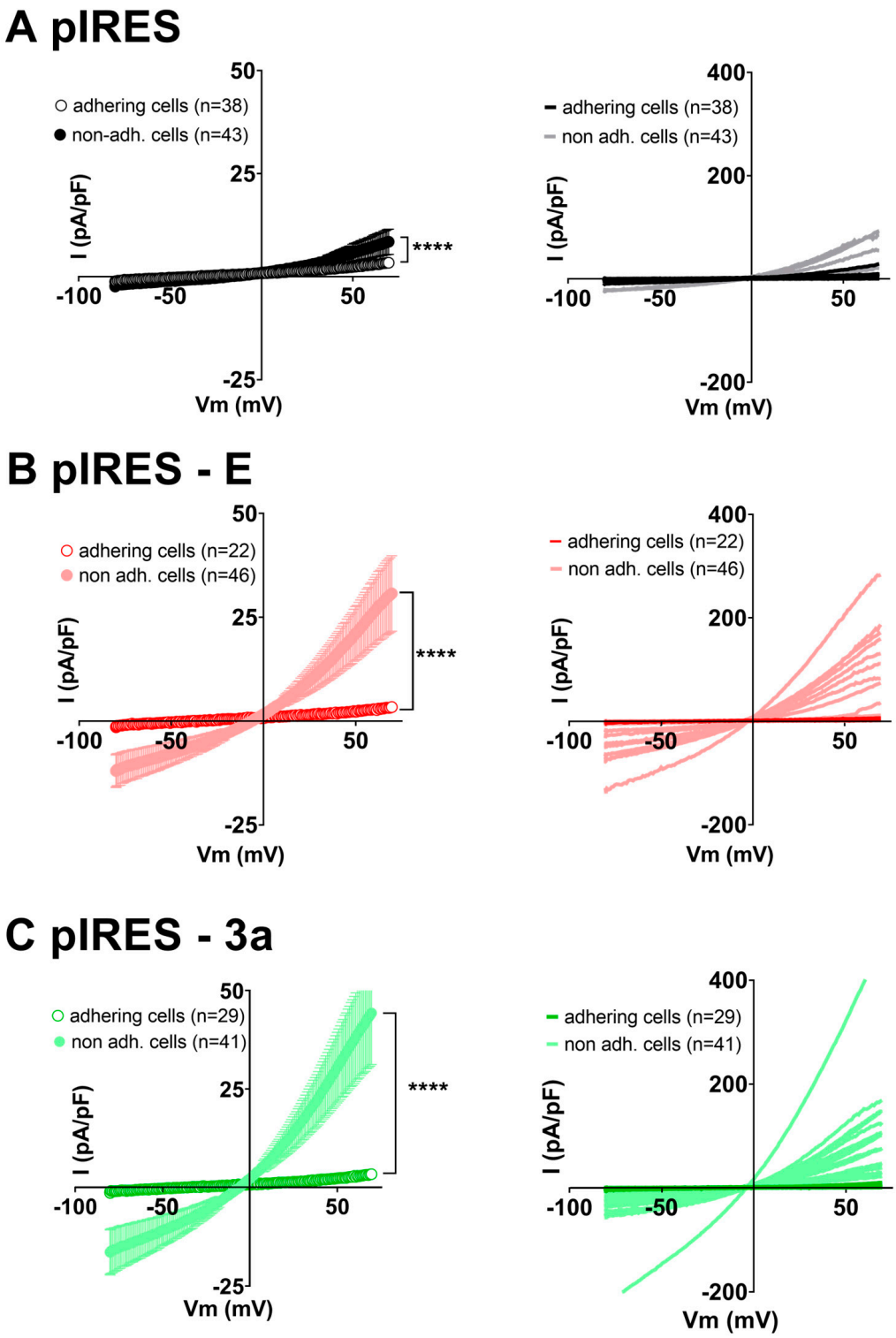

Figure 3. Expression of E or 3a protein is accompanied by outwardly rectifying currents in non-adhering CHO cells only. **Left,** average current densities (± sem) recorded during the ramp protocol in adhering (empty circles) or non-adhering (filled circles) CHO cells expressing either eGFP ((**A**), pIRES), SARS-CoV-2 E and eGFP proteins ((**B**), pIRES–E) or SARS-CoV-2 3a and eGFP proteins ((**C**), pIRES–3a). **Right,** plot of the individual adhering cells (darker color) or non-adhering cells (lighter color). ****: $p < 0.0001$, compared to adhering cells, two-way ANOVA on Ranks.

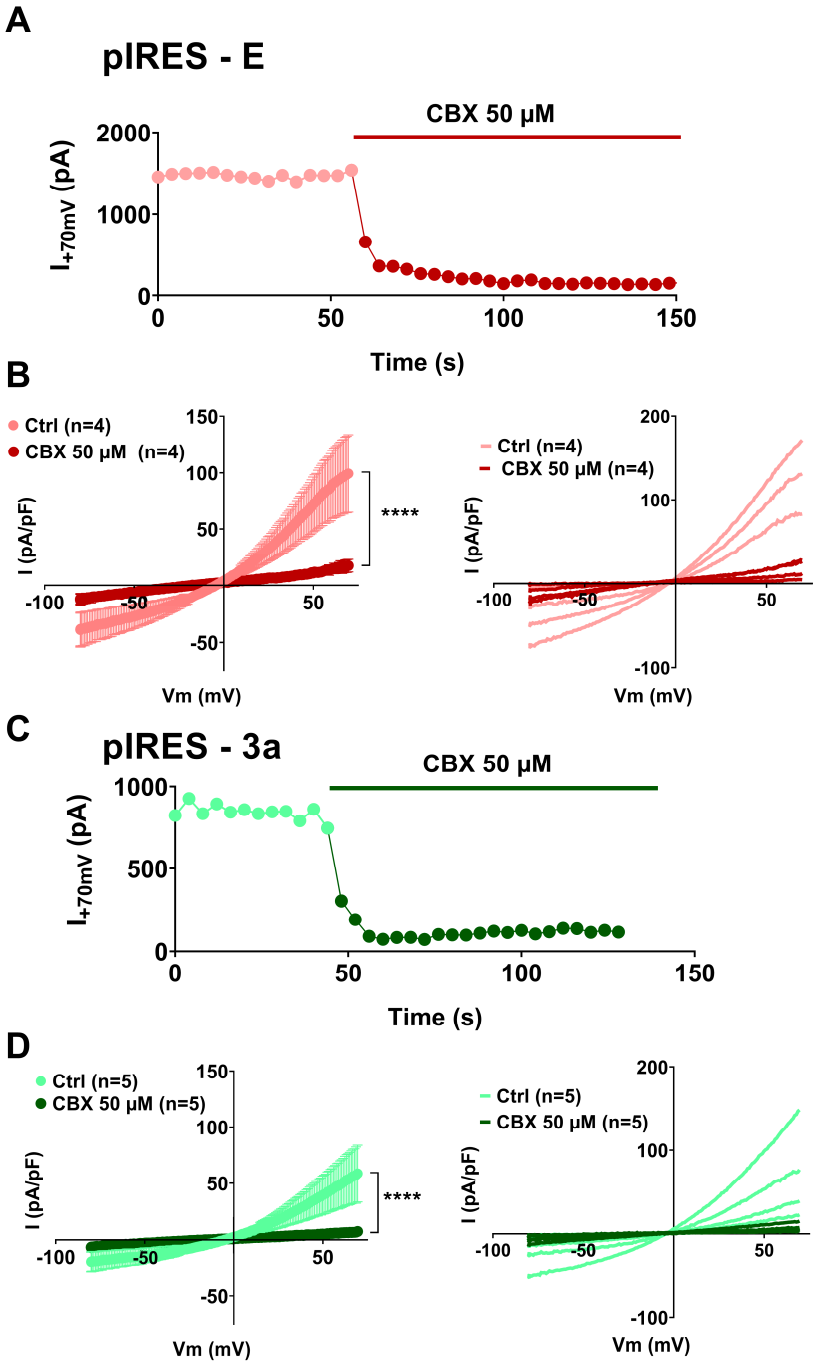

Figure 4. Currents due to E or 3a protein expression in non-adhering CHO cells are suppressed by the VRAC and pannexin inhibitor carbenoxolone (CBX). (**A**) Recording of the current amplitude in a CHO cell expressing SARS-CoV-2 E and eGFP proteins that displays large outwardly rectifying currents, in absence and presence of CBX. (**B**) **Left,** average current densities (±sem) recorded during the ramp protocol in non-adhering CHO cells, expressing SARS-CoV-2 E and eGFP proteins (pIRES–E), in absence (Ctrl, lighter color) and presence of CBX (darker color). **Right,** plot of the individual non-adhering cells in absence (lighter color) and presence of CBX (darker color). (**C**) Recording of the current amplitude in a CHO cell expressing SARS-CoV-2 3a and eGFP proteins that displays the outwardly rectifying currents, in absence and presence of CBX. (**D**) **Left,** average current densities (±sem) recorded during the ramp protocol in non-adhering CHO cells, expressing SARS-CoV-2 3a and eGFP proteins (pIRES–3a), in absence (Ctrl, lighter color) and presence of CBX (darker color). **Right,** plot of the individual non-adhering cells in absence (lighter color) and presence of CBX (darker color). ****: $p < 0.0001$, compared to Ctrl, two-way ANOVA on Ranks with repeated measures.

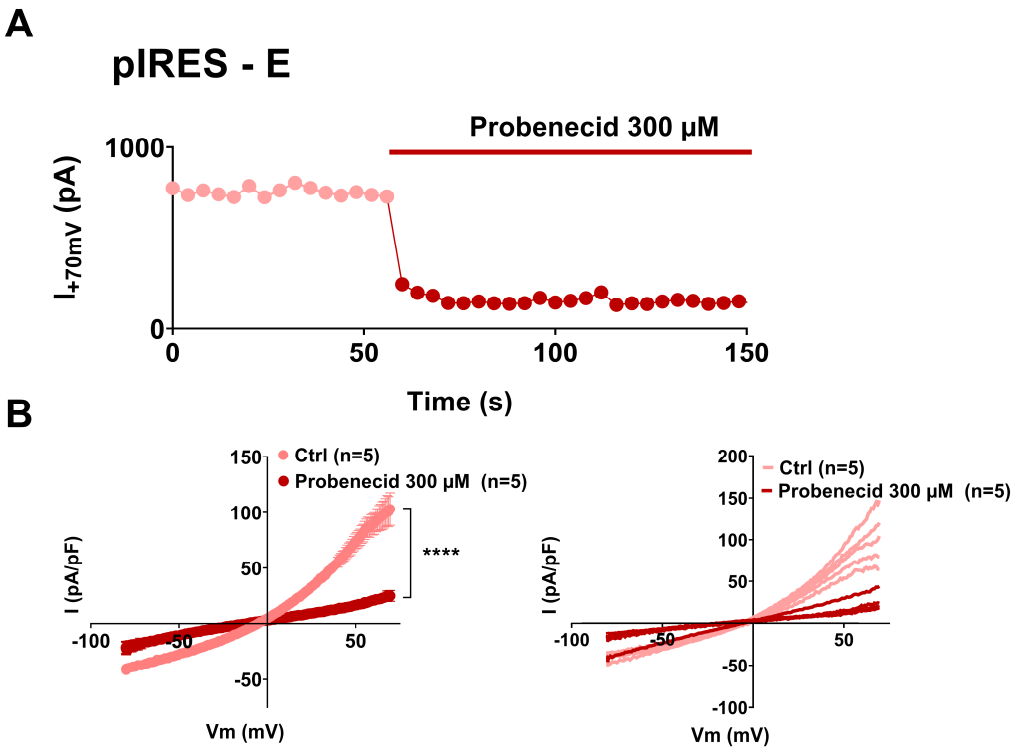

Figure 5. Currents due to E protein expression in non-adhering CHO cells are suppressed by the pannexin inhibitor probenecid. (**A**) Recording of the current amplitude in a CHO cell expressing SARS-CoV-2 E and eGFP proteins that displays large outwardly rectifying currents, in absence and presence of probenecid. (**B**) **Left**, average current densities (±sem) recorded during the ramp protocol in non-adhering CHO cells, expressing SARS-CoV-2 E and eGFP proteins (pIRES–E), in absence (Ctrl, lighter color) and presence of probenecid (darker color). **Right**, plot of the individual non-adhering cells in absence (lighter color) and presence of probenecid (darker color). ****: $p < 0.0001$ compared to Ctrl (DMSO), two-way ANOVA on Ranks with repeated measures.

We reported above (Figure 2) that deleting the last four amino acids of the E protein (Δ4) drastically reduced its pro-apoptotic effect. Cells expressing the Δ4 E protein showed an average roundness similar to cells expressing the WT protein, suggesting that deletion did not prevent its effect on cell morphology (Figure 6A and Supplementary Figure S7). Additionally, when focusing on round and non-adhering Δ4 E protein-expressing cells, we could still record large outwardly rectifying currents (5 out of 20 cells), suggesting that C-terminal deletion of E protein does not abolish the induction of pannexin currents, despite the prevention of apoptosis probed by the flow cytometry experiments (Figure 6B and Supplementary Figure S8).

We also reported in Figure 2 that the deletion of the last 10 amino acids of the 3a protein (Δ10) also decreased cell death, albeit to a lesser extent. As for E protein deletion, cells expressing the truncated 3a protein showed an average roundness similar to cells expressing the WT protein (Figure 6A and Supplementary Figure S7). Focusing on the non-adhering cells, we could still record large outwardly rectifying currents (9 out of 14 cells), suggesting that deletion of the last 10 amino acids is not sufficient to abolish the induction of pannexin-like currents (Figure 6C and Supplementary Figure S8).

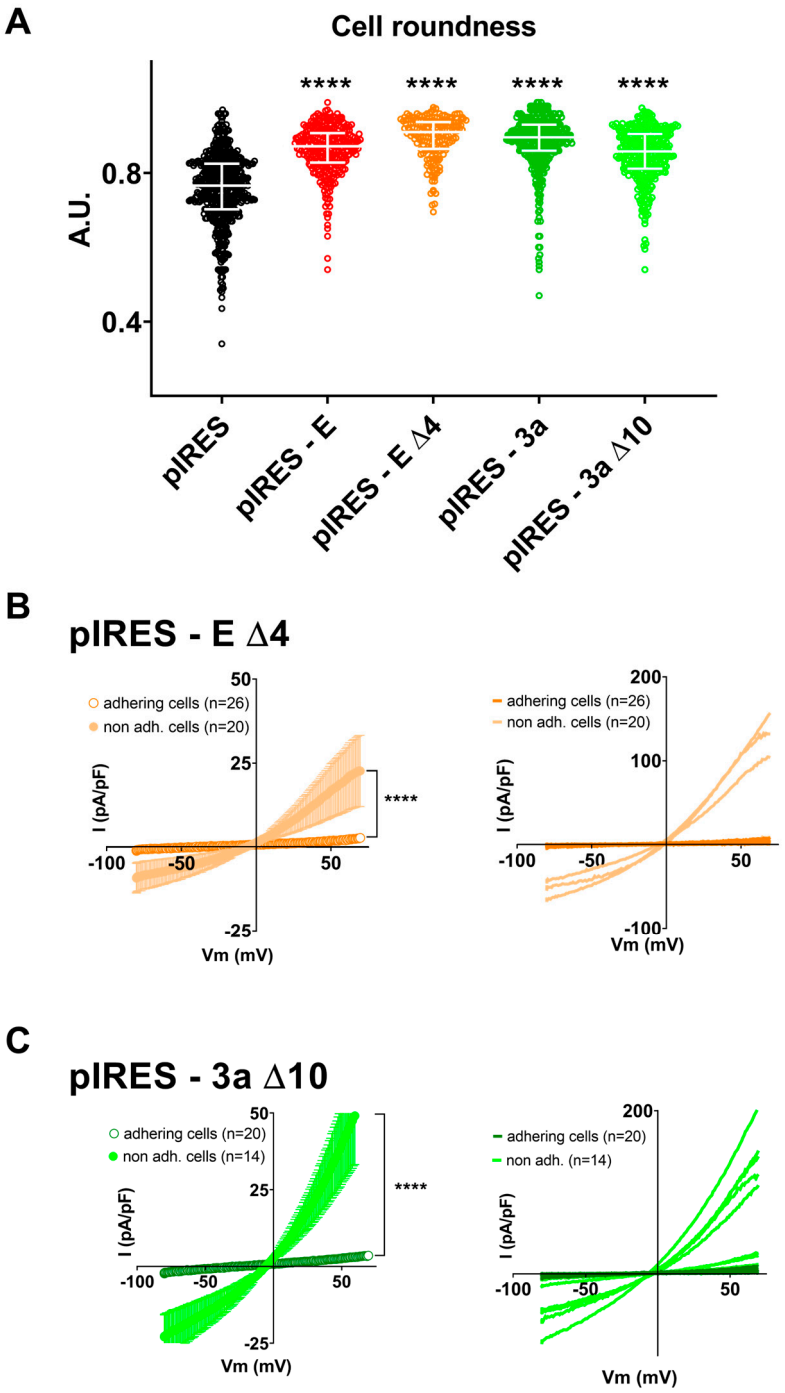

Figure 6. C-terminal deletion of E or 3a protein does not prevent cell alteration. (**A**) Cell roundness measured in CHO cells expressing eGFP (pIRES) alone or in combination with WT (pIRES–E) or the C-terminally deleted E protein (pIRES–E Δ4) or in combination with WT (pIRES–3a) or the C-terminally deleted 3a protein (pIRES–3a Δ10). Plot of individual cells, median ± interquartile range. ****: $p < 0.0001$ compared to pIRES control, Kruskal–Wallis test. (**B**) **Left,** average current densities (±sem) recorded during the ramp protocol in adhering (empty circles) or non-adhering (filed circles) CHO cells expressing the C-terminally deleted E protein (pIRES–E Δ4). **Right,** plot of the individual adhering (darker color) or non-adhering cells (lighter color). ****: $p < 0.0001$, compared to adhering cells, two-way ANOVA on Ranks. (**C**) **Left,** average current densities (± sem) recorded during the ramp protocol in adhering (empty circles) or non-adhering (filled circles) CHO cells expressing the C-terminally deleted 3a protein (pIRES–3a Δ10). **Right,** plot of the individual adhering (darker color) or non-adhering cells (lighter color). ****: $p < 0.0001$, compared to adhering cells, two-way ANOVA on Ranks.

4. Discussion

The concept that SARS-CoV E or 3a proteins could be viroporins expressed at the plasma membrane is a seductive one, as it could help the identification of new therapeutic drugs against COVID-19 by setting up a screening program based on channel activity. However, this concept is controversial, and some of the reasons that explain this controversy about the function of E and 3a proteins is likely linked to the fact that these proteins also trigger morphological alterations and/or cell death. One could imagine for instance that morphological alterations and/or cell death would be a way to activate the function of E and 3a proteins at the plasma membrane, but an alternative hypothesis could be simply that morphological alterations and/or cell death triggers endogenous cell conductances unrelated to the cell function of E and 3a viral proteins [26–29,38,42].

The only way to address these issues is to confirm that both morphological alterations and cell death are induced by E and 3a proteins, to measure plasma membrane conductance, and to characterize them to get insights on their nature and probe the pharmacological agents that would match their conductance identities. We managed to solve these issues by characterizing the membrane conductances triggered by both E and 3a proteins. The fact that both proteins trigger the same conductance independently of each other was the first indication that they could not be viroporins at the plasma membrane. The second hint was that adhering cells, whether they had a round shape or not, did not exhibit any outward conductance in spite of E or 3a protein expression. Finally, the sensitivity to carbenoxolone of the outwardly rectifying currents triggered by E or 3a proteins in non-adhering cells, but also the sensitivity to probenecid of the outwardly rectifying currents triggered by the E protein, was an indication that these viral proteins trigger cellular alterations, such as morphological changes and cell death, that are inducers of pannexin-like current. Globally, these observations remain consistent with previous observations that both E and 3a proteins are mainly localized in intracellular compartments in various cell types [14,43–47]. Therefore, it is fair to mention that we cannot fully conclude the viroporin nature of these viral proteins, as their localization in subcellular organelles prevents us from clearly testing their intrinsic potential for channel activity.

We showed that expression of either of these two proteins in CHO cells induces an increase in cell death, as quantified by flow cytometry experiments. It is likely, although we did not investigate this point in detail, that this cell death accompanies the change in cell morphology and Petri dish detachment. As such, our observation that pannexin-like currents are mainly observed in detached round-shaped cells indicates that major cell morphology changes, up to the level of surface detachment, are required for the induction of pannexin-like currents. Whatever the exact mechanism, the upregulation of pannexin channels upon cell death has been previously observed [42]. It is thus not so surprising, in fact, that other reports faced problems reporting and identifying the conductances triggered by E and 3a viral proteins. The conditions for observing them are indeed quite drastic and require examining cells that are in the combined dying and detachment process, something that is not naturally pursued by researchers, especially if one hopes to detect viroporin activity. To reconcile our data with earlier publications, we noticed that whole-cell currents observed by others after SARS-CoV-1 E or 3a protein expression in HEK 293 cells [13,19] were also very similar to pannexin currents: outwardly rectifying current with a reversal potential close to 0 mV at physiological ion concentrations indicating poor ion selectivity and an amplitude of a few 100 pA.

One possibility is that the pannexin-like currents that we observed are due to the classical caspase-induced cleavage of pannexin [48]. Intriguingly, deletion of the C-terminal PBM of E protein abolished its pro-apoptotic effect, but cell morphology alteration and the induced outwardly rectifying currents were still present. Regarding the 3a protein, deletion of its PBM domain only decreased and did not completely abolish promoted cell death, but again, cell morphology alteration and pannexin-like currents were preserved. Altogether, these results suggest that cell morphology modification and pannexin induction may be linked and that these processes are not necessarily accompanied by cell death. One has

to keep in mind that pannexin currents are activated by many stimuli in addition to cell death [48]. In particular, pannexin currents are also stretch-activated and may be enhanced in the detached cells that are undergoing major morphological alterations [26]. If pannexins are already activated by stretch, they would not be overactivated by their cleavage by caspase, which would explain the fact that E and 3a protein truncations do not prevent pannexin current, but only cell death. It may be difficult to clearly delineate the molecular nature of the outwardly rectifying currents in the absence of specific pharmacological tools [40,41,49]. Once the molecular nature of the CBX-sensitive currents is defined, it will be of interest to test if this channel is sensitive to the "viroporin" blockers that have been used elsewhere as evidence that the E/3a proteins are *bona fide* ion channels: amantadine, HMA, emodin, or xanthene [15,18,21].

5. Conclusions

In conclusion, SARS-CoV-2 native E and 3a proteins, and most likely SARS-CoV-1 ones as well, do not act as plasma membrane ion channels, but instead trigger the activity of plasma membrane pannexin channels, most likely through morphological alteration of the cells. However, our study does not rule out potential channel activity in intracellular membranes leading to morphological alterations and/or cell death. Additionally, adding a level of complexity, pannexin currents are associated with the induction of inflammation they may also be increased by cytokines such as TNF-alpha [50] and thus have been suggested as potential therapeutic targets [51–53]. Future studies will give more insights on the role of pannexin channels in COVID-19 physiopathology and treatment.

Supplementary Materials: The following supporting information can be downloaded at: https://www.mdpi.com/article/10.3390/cells12111474/s1, Figure S1: Morphology analysis of cells transfected with control pIRES, pIRES-E or pIRES-3a plasmids; Figure S2: Effects of E or 3a protein expression on early (Annexin V+, PI- in A&B) and late (Annexin V+, PI+ in C&D) cell death; Figure S3: Caspase dependence of E and 3a protein-induced cell death; Figure S4: Test of the apoptosis inducers and inhibitor in CHO cells; Figure S5: Effect of expression of E or 3a protein on membrane capacitance in adhering vs. non-adhering CHO cells; Figure S6: Expression of E or 3a protein is accompanied by outwardly rectifying currents in non-adhering CHO cells only; Figure S7: Distribution of cells roundness; Figure S8: C-terminal deletion of E or 3a protein does not prevent cell characteristic changes.

Author Contributions: Conceptualization, F.C., I.B., M.D.W. and G.L.; formal analysis, B.B.R.O.-M., M.A., B.O., I.B. and G.L.; funding acquisition, M.D.W. and G.L.; investigation, B.B.R.O.-M., M.A., B.O., I.B. and G.L.; methodology, J.M., N.B., F.S., N.E. and M.D.W.; project administration, B.B.R.O.-M., M.A. and G.L.; software, G.L.; supervision, F.C., I.B., M.D.W. and G.L.; validation, G.L.; writing—original draft, M.D.W. and G.L.; writing—review and editing, J.M., N.B., F.S., N.E., F.C., I.B., M.D.W. and G.L. All authors have read and agreed to the published version of the manuscript.

Funding: We thank the Agence Nationale de la Recherche for its financial support to the Région Pays de la Loire (ANR FLASH COVID-19–CoV2-E-TARGET) and the laboratory of excellence "Ion Channels, Science and Therapeutics" (grant No. ANR-11-LABX-0015). We acknowledge the IBISA MicroPICell facility (Biogenouest, Nantes), member of the national infrastructure France-Bioimaging supported by the French national research agency (ANR-10-INBS-04). The APC was funded by the Agence Nationale de la Recherche. The authors acknowledge the Cytocell - Flow Cytometry and FACS core facilty (SFR Bonamy, BioCore, Inserm UMS 016, CNRS UAR 3556, Nantes, France) for its technical expertise and help, member of the Scientific Interest Group (GIS) Biogenouest and the Labex IGO program supported by the French National Research Agency (n°ANR-11-LABX-0016-01).

Institutional Review Board Statement: Not applicable.

Informed Consent Statement: Not applicable.

Data Availability Statement: The data presented in this study are available on request from the corresponding author.

Acknowledgments: We thank Hugues Abriel and Jean-Sebastien Rougier (Institute of Biochemistry and Molecular Medicine, University of Bern) for fruitful discussions, support, and the critical reading of this manuscript.

Conflicts of Interest: The authors declare no conflict of interest.

References

1. Drosten, C.; Günther, S.; Preiser, W.; van der Werf, S.; Brodt, H.-R.; Becker, S.; Rabenau, H.; Panning, M.; Kolesnikova, L.; Fouchier, R.A.M.; et al. Identification of a Novel Coronavirus in Patients with Severe Acute Respiratory Syndrome. *N. Engl. J. Med.* **2003**, *348*, 1967–1976. [CrossRef]
2. Zaki, A.M.; van Boheemen, S.; Bestebroer, T.M.; Osterhaus, A.D.M.E.; Fouchier, R.A.M. Isolation of a Novel Coronavirus from a Man with Pneumonia in Saudi Arabia. *N. Engl. J. Med.* **2012**, *367*, 1814–1820. [CrossRef] [PubMed]
3. Burki, T. The Future of Paxlovid for COVID-19. *Lancet Respir. Med.* **2022**, *10*, e68. [CrossRef] [PubMed]
4. Ledford, H. Hundreds of COVID Trials Could Provide a Deluge of New Drugs. *Nature* **2022**, *603*, 25–27. [CrossRef] [PubMed]
5. Ison, M.G. Antivirals and Resistance: Influenza Virus. *Curr. Opin. Virol.* **2011**, *1*, 563–573. [CrossRef]
6. Wilson, L.; Mckinlay, C.; Gage, P.; Ewart, G. SARS Coronavirus E Protein Forms Cation-Selective Ion Channels. *Virology* **2004**, *330*, 322–331. [CrossRef]
7. Wilson, L.; Gage, P.; Ewart, G. Hexamethylene Amiloride Blocks E Protein Ion Channels and Inhibits Coronavirus Replication. *Virology* **2006**, *353*, 294–306. [CrossRef]
8. Torres, J.; Maheswari, U.; Parthasarathy, K.; Ng, L.; Liu, D.X.; Gong, X. Conductance and Amantadine Binding of a Pore Formed by a Lysine-Flanked Transmembrane Domain of SARS Coronavirus Envelope Protein. *Protein Sci.* **2007**, *16*, 2065–2071. [CrossRef]
9. Verdiá-Báguena, C.; Nieto-Torres, J.L.; Alcaraz, A.; DeDiego, M.L.; Torres, J.; Aguilella, V.M.; Enjuanes, L. Coronavirus E Protein Forms Ion Channels with Functionally and Structurally-Involved Membrane Lipids. *Virology* **2012**, *432*, 485–494. [CrossRef]
10. Nieto-Torres, J.L.; Verdiá-Báguena, C.; Jimenez-Guardeño, J.M.; Regla-Nava, J.A.; Castaño-Rodriguez, C.; Fernandez-Delgado, R.; Torres, J.; Aguilella, V.M.; Enjuanes, L. Severe Acute Respiratory Syndrome Coronavirus E Protein Transports Calcium Ions and Activates the NLRP3 Inflammasome. *Virology* **2015**, *485*, 330–339. [CrossRef]
11. Castaño-Rodriguez, C.; Honrubia, J.M.; Gutiérrez-Álvarez, J.; DeDiego, M.L.; Nieto-Torres, J.L.; Jimenez-Guardeño, J.M.; Regla-Nava, J.A.; Fernandez-Delgado, R.; Verdia-Báguena, C.; Queralt-Martín, M.; et al. Role of Severe Acute Respiratory Syndrome Coronavirus Viroporins E, 3a, and 8a in Replication and Pathogenesis. *mBio* **2018**, *9*, e02325-17. [CrossRef] [PubMed]
12. McClenaghan, C.; Hanson, A.; Lee, S.-J.; Nichols, C.G. Coronavirus Proteins as Ion Channels: Current and Potential Research. *Front. Immunol.* **2020**, *11*, 573339. [CrossRef] [PubMed]
13. Pervushin, K.; Tan, E.; Parthasarathy, K.; Lin, X.; Jiang, F.L.; Yu, D.; Vararattanavech, A.; Soong, T.W.; Liu, D.X.; Torres, J. Structure and Inhibition of the SARS Coronavirus Envelope Protein Ion Channel. *PLoS Pathog.* **2009**, *5*, e1000511. [CrossRef] [PubMed]
14. Nieto-Torres, J.L.; DeDiego, M.L.; Álvarez, E.; Jiménez-Guardeño, J.M.; Regla-Nava, J.A.; Llorente, M.; Kremer, L.; Shuo, S.; Enjuanes, L. Subcellular Location and Topology of Severe Acute Respiratory Syndrome Coronavirus Envelope Protein. *Virology* **2011**, *415*, 69–82. [CrossRef] [PubMed]
15. Toft-Bertelsen, T.L.; Jeppesen, M.G.; Tzortzini, E.; Xue, K.; Giller, K.; Becker, S.; Mujezinovic, A.; Bentzen, B.H.; Andreas, L.B.; Kolocouris, A.; et al. Amantadine Has Potential for the Treatment of COVID-19 Because It Inhibits Known and Novel Ion Channels Encoded by SARS-CoV-2. *Commun. Biol.* **2021**, *4*, 1347. [CrossRef]
16. Cabrera-Garcia, D.; Bekdash, R.; Abbott, G.W.; Yazawa, M.; Harrison, N.L. The Envelope Protein of SARS-CoV-2 Increases Intra-Golgi PH and Forms a Cation Channel That Is Regulated by PH. *J. Physiol.* **2021**, *599*, 2851–2868. [CrossRef]
17. Harrison, N.L.; Abbott, G.W.; Gentzsch, M.; Aleksandrov, A.; Moroni, A.; Thiel, G.; Grant, S.; Nichols, C.G.; Lester, H.A.; Hartel, A.; et al. How Many SARS-CoV-2 "Viroporins" Are Really Ion Channels? *Commun. Biol.* **2022**, *5*, 859. [CrossRef]
18. Breitinger, U.; Ali, N.K.M.; Sticht, H.; Breitinger, H.-G. Inhibition of SARS CoV Envelope Protein by Flavonoids and Classical Viroporin Inhibitors. *Front. Microbiol.* **2021**, *12*, 692423. [CrossRef]
19. Chan, C.-M.; Tsoi, H.; Chan, W.-M.; Zhai, S.; Wong, C.-O.; Yao, X.; Chan, W.-Y.; Tsui, S.K.-W.; Chan, H.Y.E. The Ion Channel Activity of the SARS-Coronavirus 3a Protein Is Linked to Its pro-Apoptotic Function. *Int. J. Biochem. Cell Biol.* **2009**, *41*, 2232–2239. [CrossRef]
20. Lu, W.; Zheng, B.-J.; Xu, K.; Schwarz, W.; Du, L.; Wong, C.K.L.; Chen, J.; Duan, S.; Deubel, V.; Sun, B. Severe Acute Respiratory Syndrome-Associated Coronavirus 3a Protein Forms an Ion Channel and Modulates Virus Release. *Proc. Natl. Acad. Sci. USA* **2006**, *103*, 12540–12545. [CrossRef]
21. Schwarz, S.; Wang, K.; Yu, W.; Sun, B.; Schwarz, W. Emodin Inhibits Current through SARS-Associated Coronavirus 3a Protein. *Antivir. Res.* **2011**, *90*, 64–69. [CrossRef]
22. Schwarz, S.; Sauter, D.; Wang, K.; Zhang, R.; Sun, B.; Karioti, A.; Bilia, A.; Efferth, T.; Schwarz, W. Kaempferol Derivatives as Antiviral Drugs against the 3a Channel Protein of Coronavirus. *Planta Med.* **2014**, *80*, 177–182. [CrossRef] [PubMed]
23. Miller, A.N.; Houlihan, P.R.; Matamala, E.; Cabezas-Bratesco, D.; Lee, G.Y.; Cristofori-Armstrong, B.; Dilan, T.L.; Sanchez-Martinez, S.; Matthies, D.; Yan, R.; et al. The SARS-CoV-2 Accessory Protein Orf3a Is Not an Ion Channel, but Does Interact with Trafficking Proteins. *eLife* **2023**, *12*, e84477. [CrossRef] [PubMed]

24. Ren, Y.; Shu, T.; Wu, D.; Mu, J.; Wang, C.; Huang, M.; Han, Y.; Zhang, X.-Y.; Zhou, W.; Qiu, Y.; et al. The ORF3a Protein of SARS-CoV-2 Induces Apoptosis in Cells. *Cell Mol. Immunol.* **2020**, *17*, 881–883. [CrossRef] [PubMed]
25. Xia, B.; Shen, X.; He, Y.; Pan, X.; Liu, F.-L.; Wang, Y.; Yang, F.; Fang, S.; Wu, Y.; Duan, Z.; et al. SARS-CoV-2 Envelope Protein Causes Acute Respiratory Distress Syndrome (ARDS)-like Pathological Damages and Constitutes an Antiviral Target. *Cell Res.* **2021**, *31*, 847–860. [CrossRef]
26. Bao, L.; Locovei, S.; Dahl, G. Pannexin Membrane Channels Are Mechanosensitive Conduits for ATP. *FEBS Lett.* **2004**, *572*, 65–68. [CrossRef]
27. Senthivinayagam, S.; Serbulea, V.; Upchurch, C.M.; Polanowska-Grabowska, R.; Mendu, S.K.; Sahu, S.; Jayaguru, P.; Aylor, K.W.; Chordia, M.D.; Steinberg, L.; et al. Adaptive Thermogenesis in Brown Adipose Tissue Involves Activation of Pannexin-1 Channels. *Mol. Metab.* **2021**, *44*, 101130. [CrossRef]
28. Bhat, E.A.; Sajjad, N. Human Pannexin 1 Channel: Insight in Structure–Function Mechanism and Its Potential Physiological Roles. *Mol. Cell. Biochem.* **2021**, *476*, 1529–1540. [CrossRef]
29. Osei-Owusu, J.; Yang, J.; Vitery, M.d.C.; Qiu, Z. Molecular Biology and Physiology of Volume-Regulated Anion Channel (VRAC). In *Current Topics in Membranes*; Elsevier: Amsterdam, The Netherlands, 2018; Volume 81, pp. 177–203. ISBN 978-0-12-815456-4.
30. Uchida, K.; Emoto, K.; Daleke, D.L.; Inoue, K.; Umeda, M. Induction of Apoptosis by Phosphatidylserine. *J. Biochem.* **1998**, *123*, 1073–1078. [CrossRef]
31. Crea, F.; Sarti, D.; Falciani, F.; Al-Rubeai, M. Over-Expression of HTERT in CHO K1 Results in Decreased Apoptosis and Reduced Serum Dependency. *J. Biotechnol.* **2006**, *121*, 109–123. [CrossRef]
32. Mizuguchi, H.; Xu, Z.; Ishii-Watabe, A.; Uchida, E.; Hayakawa, T. IRES-Dependent Second Gene Expression Is Significantly Lower Than Cap-Dependent First Gene Expression in a Bicistronic Vector. *Mol. Ther.* **2000**, *1*, 376–382. [CrossRef] [PubMed]
33. Choveau, F.S.; Rodriguez, N.; Ali, F.A.; Labro, A.J.; Rose, T.; Dahimène, S.; Boudin, H.; Le Hénaff, C.; Escande, D.; Snyders, D.J.; et al. KCNQ1 Channels Voltage Dependence through a Voltage-Dependent Binding of the S4-S5 Linker to the Pore Domain. *J. Biol. Chem.* **2011**, *286*, 707–716. [CrossRef] [PubMed]
34. Yu, S.P.; Kerchner, G.A. Endogenous Voltage-Gated Potassium Channels in Human Embryonic Kidney (HEK293) Cells. *J. Neurosci. Res.* **1998**, *52*, 612–617. [CrossRef]
35. Teoh, K.-T.; Siu, Y.-L.; Chan, W.-L.; Schlüter, M.A.; Liu, C.-J.; Peiris, J.S.M.; Bruzzone, R.; Margolis, B.; Nal, B. The SARS Coronavirus E Protein Interacts with PALS1 and Alters Tight Junction Formation and Epithelial Morphogenesis. *Mol. Biol. Cell* **2010**, *21*, 3838–3852. [CrossRef] [PubMed]
36. Caillet-Saguy, C.; Durbesson, F.; Rezelj, V.V.; Gogl, G.; Tran, Q.D.; Twizere, J.; Vignuzzi, M.; Vincentelli, R.; Wolff, N. Host PDZ-containing Proteins Targeted by SARS-CoV-2. *FEBS J.* **2021**, *288*, 5148–5162. [CrossRef]
37. Poon, I.K.H.; Chiu, Y.-H.; Armstrong, A.J.; Kinchen, J.M.; Juncadella, I.J.; Bayliss, D.A.; Ravichandran, K.S. Unexpected Link between an Antibiotic, Pannexin Channels and Apoptosis. *Nature* **2014**, *507*, 329–334. [CrossRef]
38. Qiu, Z.; Dubin, A.E.; Mathur, J.; Tu, B.; Reddy, K.; Miraglia, L.J.; Reinhardt, J.; Orth, A.P.; Patapoutian, A. SWELL1, a Plasma Membrane Protein, Is an Essential Component of Volume-Regulated Anion Channel. *Cell* **2014**, *157*, 447–458. [CrossRef]
39. Benfenati, V.; Caprini, M.; Nicchia, G.P.; Rossi, A.; Dovizio, M.; Cervetto, C.; Nobile, M.; Ferroni, S. Carbenoxolone Inhibits Volume-Regulated Anion Conductance in Cultured Rat Cortical Astroglia. *Channels* **2009**, *3*, 323–336. [CrossRef]
40. Dahl, G.; Qiu, F.; Wang, J. The Bizarre Pharmacology of the ATP Release Channel Pannexin1. *Neuropharmacology* **2013**, *75*, 583–593. [CrossRef]
41. Koval, M.; Schug, W.J.; Isakson, B.E. Pharmacology of Pannexin Channels. *Curr. Opin. Pharmacol.* **2023**, *69*, 102359. [CrossRef]
42. Chekeni, F.B.; Elliott, M.R.; Sandilos, J.K.; Walk, S.F.; Kinchen, J.M.; Lazarowski, E.R.; Armstrong, A.J.; Penuela, S.; Laird, D.W.; Salvesen, G.S.; et al. Pannexin 1 Channels Mediate 'Find-Me' Signal Release and Membrane Permeability during Apoptosis. *Nature* **2010**, *467*, 863–867. [CrossRef] [PubMed]
43. Yuan, X.; Li, J.; Shan, Y.; Yang, Z.; Zhao, Z.; Chen, B.; Yao, Z.; Dong, B.; Wang, S.; Chen, J.; et al. Subcellular Localization and Membrane Association of SARS-CoV 3a Protein. *Virus Res.* **2005**, *109*, 191–202. [CrossRef] [PubMed]
44. Nal, B.; Chan, C.; Kien, F.; Siu, L.; Tse, J.; Chu, K.; Kam, J.; Staropoli, I.; Crescenzo-Chaigne, B.; Escriou, N.; et al. Differential Maturation and Subcellular Localization of Severe Acute Respiratory Syndrome Coronavirus Surface Proteins S, M and E. *J. Gen. Virol.* **2005**, *86*, 1423–1434. [CrossRef]
45. Liao, Y.; Yuan, Q.; Torres, J.; Tam, J.P.; Liu, D.X. Biochemical and Functional Characterization of the Membrane Association and Membrane Permeabilizing Activity of the Severe Acute Respiratory Syndrome Coronavirus Envelope Protein. *Virology* **2006**, *349*, 264–275. [CrossRef] [PubMed]
46. Cohen, J.R.; Lin, L.D.; Machamer, C.E. Identification of a Golgi Complex-Targeting Signal in the Cytoplasmic Tail of the Severe Acute Respiratory Syndrome Coronavirus Envelope Protein. *J. Virol.* **2011**, *85*, 5794–5803. [CrossRef] [PubMed]
47. Kern, D.M.; Sorum, B.; Mali, S.S.; Hoel, C.M.; Sridharan, S.; Remis, J.P.; Toso, D.B.; Kotecha, A.; Bautista, D.M.; Brohawn, S.G. Cryo-EM Structure of SARS-CoV-2 ORF3a in Lipid Nanodiscs. *Nat. Struct. Mol. Biol.* **2021**, *28*, 573–582. [CrossRef]
48. Navis, K.E.; Fan, C.Y.; Trang, T.; Thompson, R.J.; Derksen, D.J. Pannexin 1 Channels as a Therapeutic Target: Structure, Inhibition, and Outlook. *ACS Chem. Neurosci.* **2020**, *11*, 2163–2172. [CrossRef]
49. Friard, J.; Tauc, M.; Cougnon, M.; Compan, V.; Duranton, C.; Rubera, I. Comparative Effects of Chloride Channel Inhibitors on LRRC8/VRAC-Mediated Chloride Conductance. *Front. Pharmacol.* **2017**, *8*, 328. [CrossRef]

50. Yang, Y.; Delalio, L.J.; Best, A.K.; Macal, E.; Milstein, J.; Donnelly, I.; Miller, A.M.; McBride, M.; Shu, X.; Koval, M.; et al. Endothelial Pannexin 1 Channels Control Inflammation by Regulating Intracellular Calcium. *J. Immunol.* **2020**, *204*, 2995–3007. [CrossRef]
51. Swayne, L.A.; Johnstone, S.R.; Ng, C.S.; Sanchez-Arias, J.C.; Good, M.E.; Penuela, S.; Lohman, A.W.; Wolpe, A.G.; Laubach, V.E.; Koval, M.; et al. Consideration of Pannexin 1 Channels in COVID-19 Pathology and Treatment. *Am. J. Physiol.-Lung Cell. Mol. Physiol.* **2020**, *319*, L121–L125. [CrossRef]
52. Luu, R.; Valdebenito, S.; Scemes, E.; Cibelli, A.; Spray, D.C.; Rovegno, M.; Tichauer, J.; Cottignies-Calamarte, A.; Rosenberg, A.; Capron, C.; et al. Pannexin-1 Channel Opening Is Critical for COVID-19 Pathogenesis. *iScience* **2021**, *24*, 103478. [CrossRef] [PubMed]
53. Nadeali, Z.; Mohammad-Rezaei, F.; Aria, H.; Nikpour, P. Possible Role of Pannexin 1 Channels and Purinergic Receptors in the Pathogenesis and Mechanism of Action of SARS-CoV-2 and Therapeutic Potential of Targeting Them in COVID-19. *Life Sci.* **2022**, *297*, 120482. [CrossRef] [PubMed]